A theoretical treatment of atomic short-range order and magnetism in iron-rich b.c.c. alloys

1997 J. Phys.: Condens. Matter 9 1281

(http://iopscience.iop.org/0953-8984/9/6/014)

J. Phys.: Condens. Matter **9** (1997) 1281–1300. Printed in the UK PII: S0953-8984(97)78374-7

A theoretical treatment of atomic short-range order and magnetism in iron-rich b.c.c. alloys

J B Staunton†, M F Ling‡ and D D Johnson§

† Department of Physics, University of Warwick, Coventry, UK
‡ Department of Physics, University of Monash, Australia
§ Computational Materials Science Department, Sandia National Laboratories, Livermore, CA, USA

Received 4 October 1996

Abstract. We use a 'first-principles' concentration-wave approach based on a finite-temperature, electronic density-functional, mean-field, grand potential of the random alloy to investigate the atomic short-range order (ASRO) in some **Fe**V and **Fe**Al solid solutions in both ferromagnetic and paramagnetic phases. Thermally induced spin fluctuations are modelled in terms of local moments on the Fe sites. This picture produces satisfactory estimates of all of the alloys' Curie temperatures, T_c. We compare our calculations with the ASRO deduced from neutron and x-ray diffuse scattering measurements on single crystals carried out either *in situ* at or quenched from temperatures above and below T_c. Our calculations describe the measured ASRO well. Both alloy systems exhibit B2-type ordering correlations in their paramagnetic states which strengthen in the case of **Fe**V and weaken for **Fe**Al as the temperature is lowered into the ferromagnetic state. We extract electronic mechanisms for these effects. The ASROs of the ferromagnetic alloys also show intensity around (1/2, 1/2, 1/2) which is traced to a Fermi surface feature and may be a precursor to the DO_3 ordering in **Fe**Al. Finally, suggestions for further polarized neutron, *in situ* measurements are made.

1. Introduction

An analysis of the types of ordered structures that iron alloys form inevitably includes a consideration of their magnetic properties. Since the Curie temperatures of iron-rich b.c.c. alloys are often comparable with their compositional ordering (or phase segregation) transition temperatures, the magnetic state can affect the type of chemical order formed and its dependence on its thermal history.

This is brought about by the effect of magnetic order upon the electronic structure of the alloy. Long-range magnetic order establishes a 'global' spin polarization of the electronic structure which typically produces different electronic mechanisms for arranging the atoms than those set up by the paramagnetic alloy, which has no 'global' axis of spin polarization. The actual nature of the paramagnetic state, e.g. whether 'local-moment'-like spin fluctuations are present or not, has ramifications for the electronic structure. These magnetic effects, which are usually assumed to be subtle are, therefore, important for the understanding of the origin of atomic ordering in these alloys.

We approach this topic via an investigation of the atomic short-range order (ASRO) present in two iron alloy systems, **Fe**Al and **Fe**V, at (or rapidly quenched from) temperatures T_0 above any compositional ordering temperature. We find the ASRO to be sensitive to

0953-8984/97/061281+20$19.50

whether T_0 is above or below the alloys' magnetic Curie temperatures T_c and also to the details of the paramagnetic state.

Following some early neutron data from powdered crystal samples [1], Cable *et al* [2] carried out some measurements at room temperature of the scattering from a single crystal of $Fe_{87}V_{13}$ along the [1, 0, 0], [1, 1, 0], and [1, 1, 1] symmetry directions. A saturating magnetic field was applied parallel to the scattering vector which extinguished the magnetic scattering enabling the nuclear scattering to be extracted from the data. Although the sample had been annealed at and quenched rapidly from 1270 K, above the alloy's Curie temperature of 1180 K, the effective temperature for the ASRO was estimated to be 900 K. Recently Pierron-Bohnes *et al* [3] overcame the problem of making such an estimate by carrying out experiments on a $Fe_{80}V_{20}$ single crystal *in situ*. The measurements were carried out at temperatures above the sample's Curie temperature T_c. They found qualitative differences in their interpretation of their measurements on the alloy in its paramagnetic state from those of Cable *et al* on their ferromagnetic alloy. Pierron-Bohnes *et al* did not, however, account for the contribution of magnetic scattering to their data.

Here we describe our calculations of the ASRO of both ferromagnetic and paramagnetic $Fe_{87}V_{13}$ and also paramagnetic $Fe_{80}V_{20}$. We also outline our calculations of the magnetic correlations present in the paramagnetic alloys together with estimates of the Curie temperatures. Our objective is to produce an interpretation of both groups' experiments as well as investigating the effect of magnetic order upon ASRO in these systems.

Iron-rich Fe–Al alloys are promising candidates for the basis of a new family of superalloys and have therefore attracted the attention of materials scientists [4]. McKamey *et al* [5] and others have reviewed their properties together with the effects of the addition of impurities. One limiting factor on the use of these alloys seems to be their poor ductility above 900 K. It is therefore appropriate to gain an understanding of the processes which govern how the atoms order. Their high Curie temperatures ($\approx$900 K) imply that the degree of magnetic order is liable to be an important factor. These alloys are consequently also interesting test-beds for theories which treat the interplay between magnetic and chemical ordering. The phase diagram [6] shows that on cooling from the melt, paramagnetic $Fe_{80}Al_{20}$ forms a solid solution. The alloy becomes ferromagnetic at 935 K and then forms an apparent DO_3 ordered phase at about 670 K. An alloy with just 5% more aluminium orders into a B2 phase from the paramagnetic state at roughly 1000 K and orders into a DO_3 phase at lower temperatures. In this paper, we compare our ASRO calculations for **Fe**Al with data from a series of x-ray and neutron scattering experiments.

2. Exchange-split electronic structure and compositional ordering in alloys

Before describing the results of our calculations we highlight some aspects of the electronic structure of magnetic metallic alloys which are relevant to their ordering, or phase segregation, propensities. Evidently the rigidly exchange-split, spin-polarized bands usually associated with Stoner theory are plainly a special case for ferromagnetic elemental metals and are inapplicable to most magnetic intermetallic compounds and compositionally disordered alloys, as demonstrated in many studies [7, 8].

Consider two elemental d-electron densities of states in schematic rectangular box form centred on energy levels ε_A and ε_B for elements A and B respectively. Each has a width W. If $\varepsilon_A - \varepsilon_B \gg W$, then the density of states of the alloy formed from A and B will be 'split band' in nature. On the other hand, if $\varepsilon_A - \varepsilon_B \ll W$, then the alloy's electronic structure can be categorized as 'common-band'-like. There is now large-scale hybridization between states associated with the A and B atoms and each site in the alloy is nearly charge

neutral as an individual ion is efficiently screened by the metallic response function of the alloy [9]. Of course, the actual interpretation of the detailed electronic structure involving many bands is often a complicated mixture of these two models. In both cases, half-filling of the bands lowers the total energy of the system with respect to the phase-separated case [10, 11].

When magnetism is added to the problem, an extra ingredient, namely, the difference between the exchange fields associated with each type of atomic species, is supplied. For majority-spin electrons, the rough measure of the degree of 'split-band' or 'common-band' nature of the density of states is governed by $(\varepsilon_A^{\uparrow} - \varepsilon_B^{\uparrow})/W$, with a similar measure $(\varepsilon_A^{\downarrow} - \varepsilon_B^{\downarrow})/W$ for the minority-spin electrons. If the exchange fields differ to any large extent, then, for electrons of one spin polarization, the bands are common-band-like, whilst for the others a 'split-band' annotation is likely to be more appropriate. The cumulative result is a spin-polarized electronic structure which is not set up by a rigid exchange splitting. Williams *et al* [12] have coined the phrase 'covalent magnetism' to describe this behaviour, and an example of this effect in disordered Ni–Fe and Fe–V has been presented by Johnson *et al* [13].

Hund's rules dictate that it is frequently energetically favourable for the majority-spin d states to be full, and there are many examples, such as nickel-rich nickel–iron alloys [13, 15, 14], where, at the cost of a small charge transfer, this is accomplished. There are many other systems which are not strong ferromagnets in this sense but possess an analogous attribute. In these materials, the chemical potential is pinned in a deep valley in either the majority- or minority-spin density of states.

As a metallic magnet is heated up, spin fluctuations are induced which eventually destroy the long-range magnetic order and, hence, the 'global' spin polarization of the system. These collective electron modes interact as the temperature is raised and are dependent upon and can affect the underlying electronic structure. In many materials such spin fluctuations can be modelled by 'local moments' which produce local magnetic fields on the lattice sites. The moments are assumed to vary their orientations slowly on the time-scale of the electronic motions [16] and to be self-consistently maintained by them. The average over the local moments' orientations produces zero overall magnetization in the paramagnetic state, but, nonetheless, the electronic structure is affected by this local-moment disorder.

An *ab initio* implementation of this local-moment picture, in which the electronic structure and spin fluctuations are mutually consistent, has been set up within a mean-field (MF) framework [17] (the so-called disordered-local-moment (DLM) approach) improved by the inclusion of Onsager cavity fields [18] and represents a well-defined stage of approximation. It gives a fair account of the paramagnetic states of Fe, Ni and **Cu**Mn alloys [19]. We use this theory in this paper in the version generalized for alloys [20].

An early prediction [17] from the DLM model of the paramagnetic state of b.c.c. iron described a 'local' exchange splitting or spin polarization of its electronic structure, the size of which varied sharply as a function of wavevector ($\boldsymbol{k}$) and energy. This feature is present in most other 'local-moment' descriptions of the paramagnetic states of ferromagnetic metals. This local exchange splitting establishes the local moment. At some points where the bands are flat, the splitting would be the same size as that in the low-temperature magnetically ordered state, whereas, at other points of greater dispersion, the splitting would vanish entirely. While this general feature has been observed in the small number of photoemission and inverse photoemission experiments on this topic [21], in detail the DLM electronic structure is less 'locally exchange split' than that observed for the small region of $\boldsymbol{k}$-space probed by the experiments. Using a parametrized tight-binding model, Haines *et al* [22] concluded that a modest degree of SRO among the local moments is required for closer

agreement between theory and experiment for pure iron.

In this paper, we analyse the atomic ordering of the two iron-rich alloy systems and indicate how it is affected by the change in the electronic structure from being 'locally' exchange split to being 'globally' exchange split as the temperature is lowered through the Curie temperature. In alloys, the electronic interactions which support such thermal, local-moment, spin fluctuations at high temperatures in the paramagnetic state are also responsible for determining the nature of the compositional ordering there. Moreover, with the onset of long-range magnetic order at lower temperatures, the electronic structure takes on different features which can provoke a different type of compositional order. In addition, both of these cases can produce atomic arrangements which are markedly different from what would be set up by the alloy's electronic structure if it possessed no exchange splitting at all, local or otherwise. This would be the case of a paramagnetic state of a ferromagnetic material if it lost its magnetization via Stoner particle–hole excitations.

In the next section we briefly summarize the relevant aspects of the theory for atomic short-range order in alloys and its dependence on their magnetic states. Full details have been published elsewhere [23, 20, 24]. The following two sections describe the application of this theory to the two iron alloy systems in which attributes of the electronic structure highlighted above are used to interpret the full 'first-principles' calculations of the atomic short-range order. The calculated ASROs are used to make the first parameter-free comparisons with available diffuse neutron and x-ray scattering data. The final section draws some conclusions from the work and proposes some additional experimental measurements.

3. Atomic short-range order in alloys

Atomic ordering in alloys is usefully described in terms of 'concentration waves' [25]. As the atoms begin to arrange themselves as the alloy cools, the probability of finding a particular atomic species occupying a lattice site, namely the site-dependent concentration, varies from site to site and traces out a static concentration wave. For example, the well-known Cu_3Au and CuZn ordered alloys are characterized by a concentration wave with wavevector $\boldsymbol{q} = (0, 0, 1)$ on f.c.c. and b.c.c. crystal lattices, respectively. On the other hand, an infinitely long-wavelength concentration wave, i.e. $\boldsymbol{q} \to 0$, describes an alloy which phase segregates at low temperatures. The central result of concentration-wave theory is that $S^{(2)}(\boldsymbol{q}, T)$, the lattice Fourier transform of the Ornstein–Zernicke direct correlation function,

$$S^{(2)}_{jk} = \left.\frac{\delta^2 \Omega\{c_i\}}{\delta c_j \, \delta c_k}\right|_{\{c_i = c\}} \tag{1}$$

provides direct information on the stability of the randomly disordered alloy to concentration fluctuations at a given temperature T [26]. $\Omega\{c_i\}$ is the electronic grand potential for an inhomogeneous configuration specified by the set of site concentrations $\{c_i\}$. Experimentally the instability of the disordered phase to ordering may be seen in electron, x-ray or neutron scattering measurements. These are directly related to the Warren–Cowley short-range-order parameter, $\alpha(\boldsymbol{q}, T)$, which in turn is related to $S^{(2)}(\boldsymbol{q}, T)$ (for a binary alloy) through

$$\alpha(\boldsymbol{q}, T) = \frac{1}{(1 - \beta c(1 - c) S^{(2)}(\boldsymbol{q}, T))}. \tag{2}$$

Our purpose is to compare the topology and magnitude of $\alpha(\boldsymbol{q}, T)$ in scattering vector $\boldsymbol{q}$-space directly with that extracted from scattering data rather than to make a comparison at the level of fitted real-space, Warren–Cowley parameters. We also provide representations

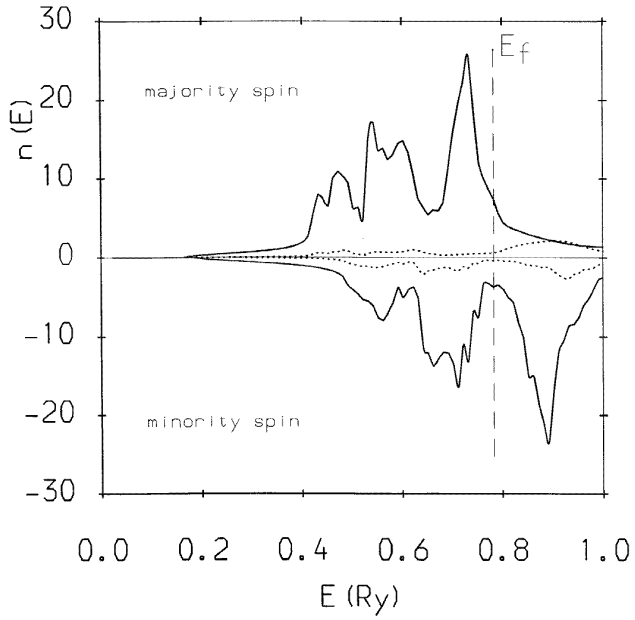

(a)

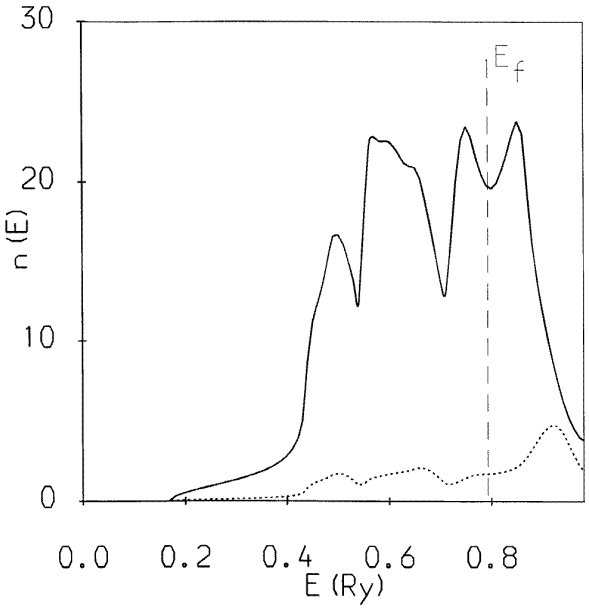

(b)

Figure 1. (a) The majority- and minority-spin, compositionally averaged densities of states of ferromagnetic $Fe_{87}V_{13}$ and its resolution into components weighted by concentration, in units of states Ryd^{-1}/(atom spin). (b) The compositionally averaged density of states of paramagnetic (DLM) $Fe_{87}V_{13}$ and its resolution into components associated with Fe (solid) and V (dotted) sites weighted by concentration, in units of states Ryd^{-1}/(atom spin).

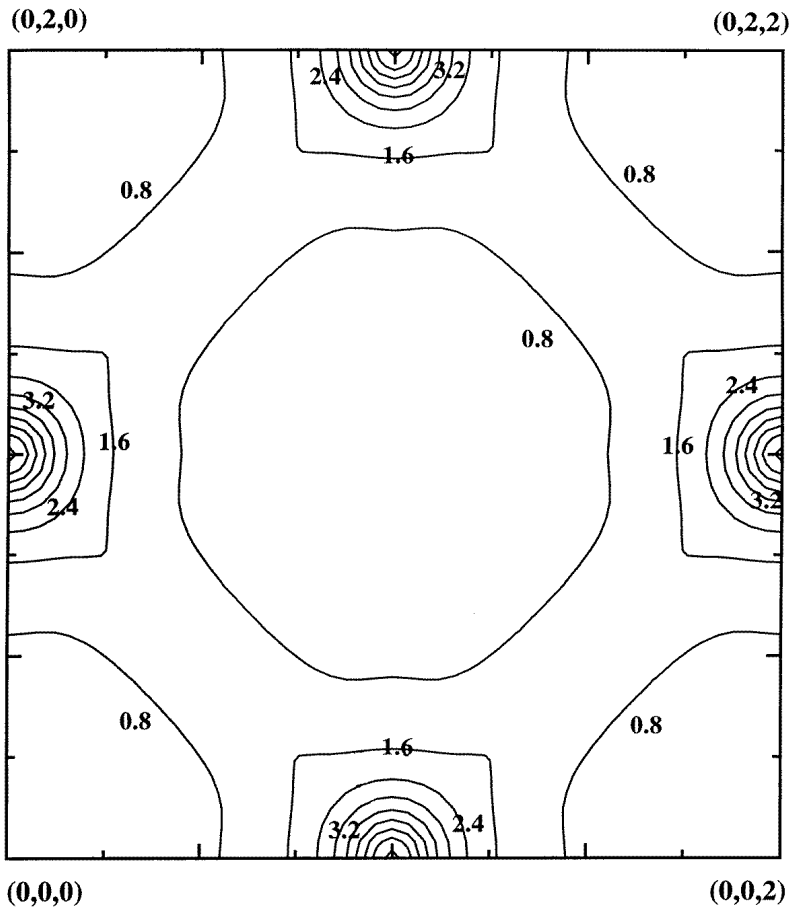

(a)

Figure 2. (a) The ASRO ($\alpha^{DLM}(\boldsymbol{q}, T)$) for the $(1, 0, 0)$ plane for ferromagnetic $Fe_{87}V_{13}$ at 200 K above the theoretical spinodal temperature of 1650 K in Laue units. (b) As (a), but for the $(1, \bar{1}, 0)$ plane.

of the direct correlation function $S^{(2)}(\boldsymbol{q}, T)$ in terms of real-space quantities $S_{ij}^{(2)}$ in order to give an impression of its range. It should be strongly emphasized that the $S_{ij}^{(2)}$s are not effective pairwise interactions that would, say, appear in Ising representations used in inverse Monte Carlo [27] or CVM analyses of the experimental data [28].

Elsewhere [23] we have described in detail how $S^{(2)}(\boldsymbol{q}, T)$ may be calculated from a 'first-principles', mean-field approach. We start from a SCF-KKR-CPA description of the electronic structure of the high-temperature, compositionally disordered state in which charge-correlation effects are included [29]. The coherent-potential approximation (CPA) is used to average over the compositional fluctuations. All electronic effects are included, apart from those causing lattice displacements. In particular, the alteration of charge that occurs as the atoms are rearranged is fully incorporated, i.e. charge-transfer effects are included. From the same basis, an expression for the wavevector-dependent, static, para-

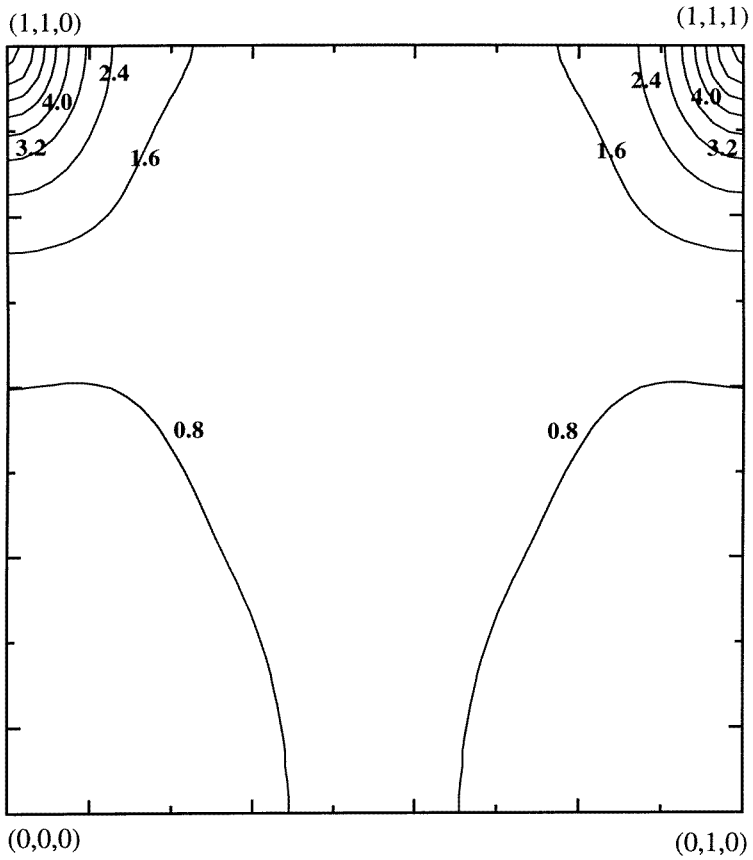

(b)

Figure 2. (Continued)

magnetic spin susceptibility for the alloy $\chi(\boldsymbol{q}, T)$ can be set up [20] and used to describe the magnetic correlations in the paramagnetic state, $M(\boldsymbol{q}, T) = 3k_B T \chi(\boldsymbol{q}, T)$, via the fluctuation-dissipation theorem.

The CPA is also used to average over the orientational disorder of the local moments in the DLM paramagnetic states [18]. We then investigate the ASRO set up by an electronic structure of the paramagnetic phases of the alloys, which support, and are affected by, the DLM spin fluctuations together with that formed by paramagnetic phases with no local moments. We compare both results with the ASRO from the alloys' ferromagnetic states [20, 24].

4. Atomic short-range order of $Fe_{87}V_{13}$

Iron-rich Fe–V alloys have several attributes which make them suitable systems in which to investigate both ASRO and magnetism. Firstly, their Curie temperatures ($\approx$1000 K) lie in a range which makes it possible to compare and contrast the ASRO set up by both the ferromagnetic and paramagnetic states. The large difference between the coherent neutron

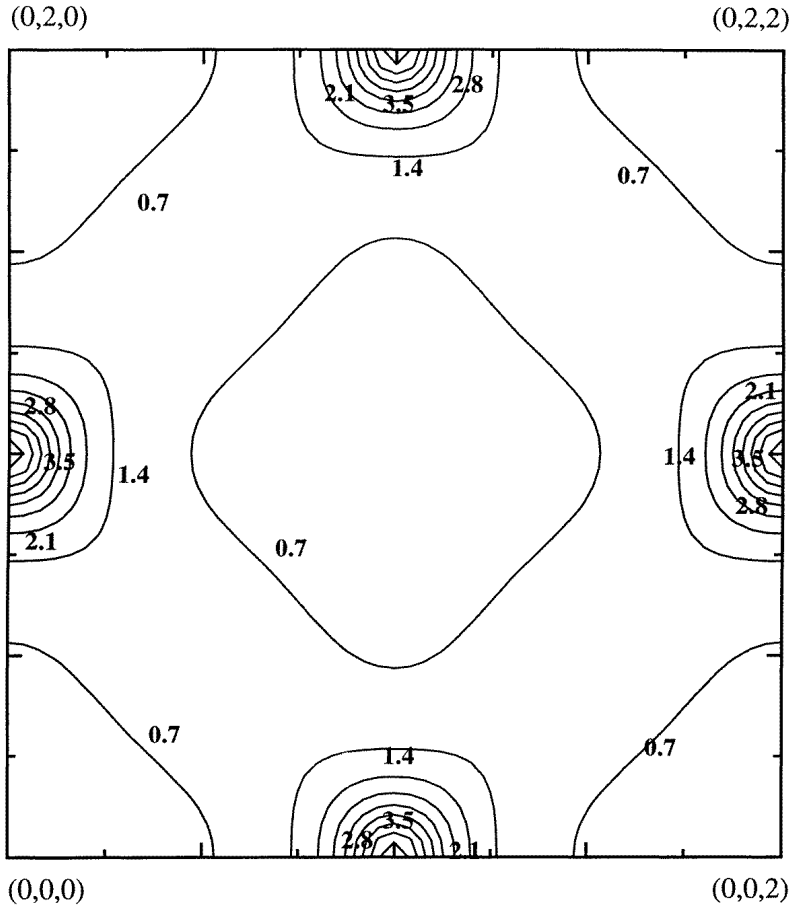

(a)

Figure 3. (a) The ASRO ($\alpha^{DLM}(\boldsymbol{q}, T)$) for the (1, 0, 0) plane for paramagnetic (DLM) $Fe_{87}V_{13}$ at 200 K above the theoretical spinodal temperature of 1080 K in Laue units. (b) As (a), but for the $(1, \bar{1}, 0)$ plane.

scattering lengths, $b_{Fe} - b_V \approx 10$ fm, and a small size effect associated with alloying make them good candidates for neutron diffuse scattering experimental analyses as discussed in the introduction.

Figure 1 of the paper by Cable *et al* [2] shows the neutron scattering cross sections along three symmetry directions, measured in the presence of a saturating magnetic field for a $Fe_{87}V_{13}$ single crystal quenched from within the ferromagnetically ordered state. The structure of the curves is attributed to nuclear scattering connected with ASRO, $c(1-c)(b_{Fe} - b_V)^2\alpha(\boldsymbol{q})$. The most intense peaks occur at (1, 0, 0) and (1, 1, 1), indicative of a β-CuZn (B2) ordering tendency. There is also substantial intensity in the form of a double-peak structure at around $(1/2, 1/2, 1/2)$. In an earlier publication [30], we showed how our ASRO calculations for *ferromagnetic* $Fe_{87}V_{13}$, which included only band-filling effects from the electronic structure [23], could reproduce all the details of the data. For

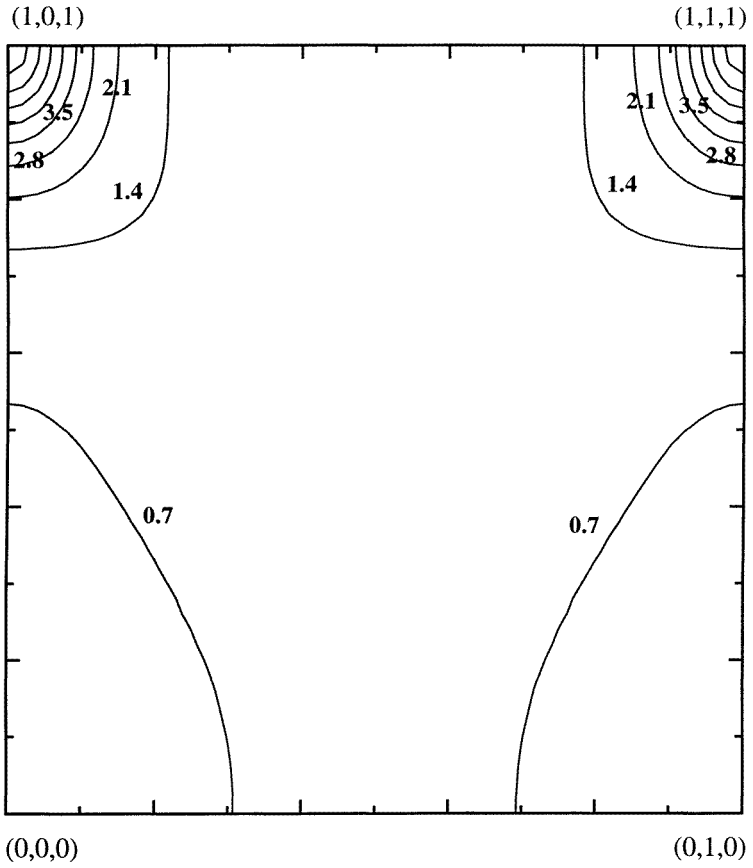

(b)

Figure 3. (Continued)

this alloy, the chemical potential is pinned in a trough of the minority-spin density of states (figure 1(a)), so there is substantial hybridization between states associated with the two different atomic species, and the tendency to order is governed principally by the majority-spin electrons. These states are roughly half-filled to produce the strong ordering tendency [30]. The calculations also showed that part of the structure at around $(1/2, 1/2, 1/2)$ could be traced back to the majority-spin Fermi surface of the alloy.

Figures 2(a) and 2(b) show contour plots of $\alpha(\boldsymbol{q})$ in the $(1, 0, 0)$ and $(1, \bar{1}, 0)$ planes on the basis of our all-electron theory assuming a ferromagnetic state for the alloy. The details are the same as before, although the estimate of the spinodal compositional ordering temperature, T_{comp} (1570 K compared to 950 K) is larger owing to the inclusion of charge-rearrangement effects. In due course when the consequences of lattice displacements are also included into the theory, we expect this estimate to decrease as the one effect offsets the other. We can fit the direct correlation function $S^{(2)}(\boldsymbol{q})$ in terms of real-space parameters:

$$S^{(2)}(\boldsymbol{q}) = S_0^{(2)} + \sum_n \sum_{i \in n} S_n^{(2)} \exp(\mathrm{i}\boldsymbol{q} \cdot \boldsymbol{R}_i).$$

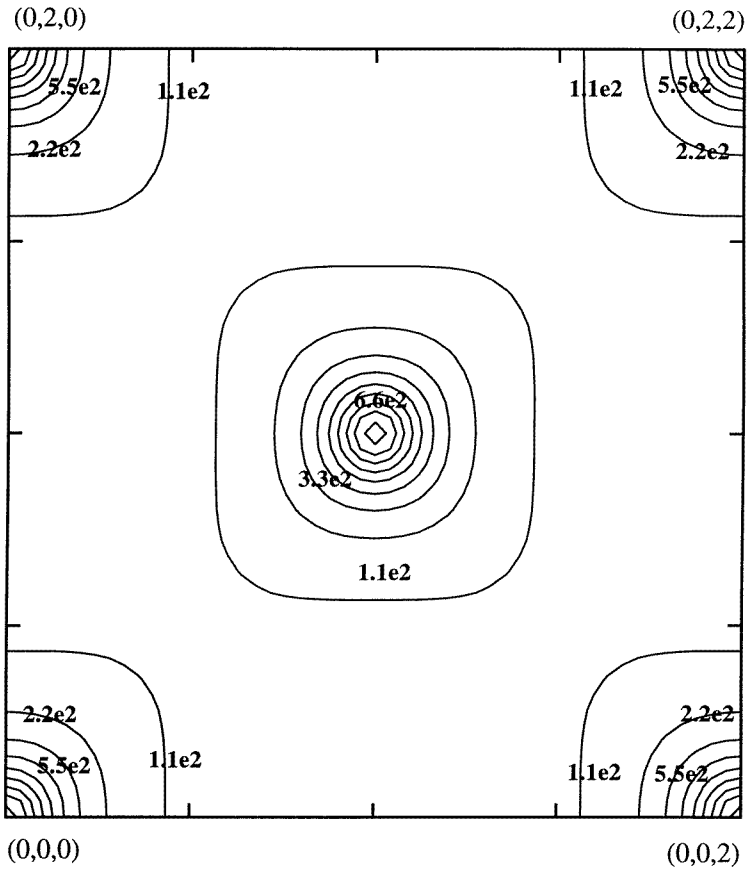

Figure 4. The paramagnetic susceptibility of (DLM) $Fe_{80}V_{20}$ at 200 K above the Curie temperature of 950 K in units of $4\mu_B^2$ Ryd for the $(1, 0, 0)$ plane.

The fit is dominated by the first two parameters which determine the large peak at $(1, 0, 0)$. However, the fit also shows that there is a long-range component that, we have found, is derived from the Fermi surface effect. $S^{(2)}_{n=1,2,\ldots}$ is shown for the first nine shells in table 1. $S^{(2)}_0 = -16.5$ mRyd describes the effect of the Onsager cavity-field correction [23]. Also shown is the Cable *et al* real-space fit of $\beta V(\boldsymbol{q})$ (assuming an effective temperature of 900 K) extracted from their measured $\alpha(\boldsymbol{q}) = A[1-c(1-c)\beta V(\boldsymbol{q})]^{-1}$ (A is a normalization constant). As in our calculation, these parameters also show large negative values for the first two shells followed by a weak long-ranged tail.

Cable *et al* claimed that the effective temperature for at least part of the sample was indeed below its Curie temperature. To investigate this we carried out calculations for the ASRO of paramagnetic (DLM) $Fe_{87}V_{13}$ and the details are shown in figures 3(a) and 3(b). Once again, the largest peaks are located at $(1, 0, 0)$ and $(1, 1, 1)$ but a careful scrutiny finds less structure around $(1/2, 1/2, 1/2)$ than for the ferromagnetic alloy. The ordering correlations are also weaker in this state—the spinodal temperature being 1060 K. For the paramagnetic DLM state, the local exchange splitting also pushes many anti-bonding states above the chemical potential ν although ν is no longer wedged in a valley in the density

Table 1. For Fe–V alloys, the calculated direct pair correlations, $S_n^{(2)}$, and the pairwise functions extracted from experiment expressed (in mRyd) in real space as a function of near-neighbour shells. The value $S_0^{(2)}$ reflects the Onsager corrections. Both ferromagnetic (FM) and paramagnetic (PM) results of our calculations are shown for $Fe_{87}V_{13}$ and compared with the data of Cable *et al* [2]. The values extracted by Pierron-Bohnes *et al* [3] from a real-space analysis of their data on a paramagnetic $Fe_{80}Al_{20}$ alloy using the CVM are also quoted.

	$S^{(2)}$	Cable *et al*	$S^{(2)}$	Pierron-Bohnes *et al*	
Shells	FM	FM	DLM-PM	1473 K PM	1133 K PM
0	−16.5		−7.6		
1	−14.2	−4.9	−7.5	−2.40	−2.88
2	−5.8	−3.1	−3.0	+ 1.04	+ 0.36
3	−1.7	+ 0.6	+ 1.5	+ 0.84	+ 1.36
4	+ 0.3	+ 0.0	+ 0.3	+ 0.36	+ 0.36
5	+ 2.0	+ 0.0	+ 2.0	+ 0.44	+ 0.56
6	−0.8	−0.1	+ 0.0	—	—
7	−0.5	+ 0.1	+ 0.1	—	—
8	−0.8	+ 0.3	+ 0.2	—	—
9	−0.5	+ 0.0	+ 0.1	—	—

of states (figure 1(b)). This produces a compositional ordering mechanism that is similar to, although weaker than, that for the ferromagnetic alloy. For comparison, we also quote the DLM-PM $S_n^{(2)}$s in table 1 which show that the long-ranged tail is reduced. Evidently the 'local-moment' spin-fluctuation disorder has broadened the alloy's Fermi surface and lessened its effect upon the ASRO.

Figure 3 in the paper by Pierron-Bohnes *et al* [3] shows their measured neutron diffuse scattering intensities from $Fe_{80}V_{20}$ in its paramagnetic state at 1473 K and 1133 K (the Curie temperature is 1073 K) for scattering vectors in both the $(1, 0, 0)$ and $(1, -1, 0)$ planes, following a standard correction for instrumental background and multiple scattering. There is maximal intensity at about $(1, 0, 0)$ and $(1, 1, 1)$ and no subsidiary structure at about $(1/2, 1/2, 1/2)$. Our calculations of the ASRO of paramagnetic $Fe_{80}V_{20}$, which are very similar to those for $Fe_{87}V_{13}$ shown in figures 3, are consistent with these features.

Although no experimental data are given near $\boldsymbol{q} = 0$, the fit to the experimental data (which the authors assume is entirely nuclear in origin) also shows substantial intensity at $\boldsymbol{q} = 0$ and equivalent reciprocal-lattice points. This would suggest that both ordering and clustering tendencies coexist in the system. This aspect is not found in either our calculations or the data of Cable *et al*. Pierron-Bohnes *et al* then make an estimate of the incoherent contribution and extract effective pairwise interactions by the inverse cluster variation method [28]. These are also shown in table 1 for 1473 K and at 1133 K for the first five shells. Although not strictly comparable, these are qualitatively different, both in magnitude and form, from our $S_n^{(2)}$s and the V_ns of Cable *et al*. The growth of magnetic short-range order with decreasing temperature is held responsible for the striking difference between the interactions extracted from the two sets of data. We suggest instead that it is in part an artefact of the fitting procedure [31] and in part a consequence of not subtracting the effect of magnetic scattering from the data.

Although there are no experimental data presented by Pierron-Bohnes *et al* for the regions around reciprocal-lattice vectors, it is noteworthy that magnetic scattering will produce peaks there. These are consequences of the fluctuating local moments on the iron atoms. In figure 4, we show contour plots of the calculated paramagnetic spin susceptibility

for $Fe_{80}V_{20}$ at 1150 K which is related to the magnetic component of the neutron scattering. Ferromagnetic correlations are shown which grow in intensity as T is reduced. These lead to an estimate of $T_c = 980$ K, which agrees well with the measured value of 1073 K. (The value of T_c for $Fe_{87}V_{13}$ of 1075 K also compares well with the measured value of 1180 K.) We note that the estimate given by Pierron-Bohnes *et al* of the integrated intensity, i.e. $\int \alpha(\boldsymbol{q})\ \mathrm{d}\boldsymbol{q}$, deviates from 1 by a larger margin for the data taken close to T_c (1.25 for 1133 K, 1.11 for 1473 K) [32]. These discrepancies can be put down in part to a contribution to the cross sections from magnetic scattering.

We also examined the importance of modelling the paramagnetic alloy in terms of local moments by repeating the calculations of ASRO assuming a 'Stoner' paramagnetic state in which there are no local moments and hence zero exchange splitting of the electronic structure, local or otherwise. The maximum intensity is now found at about $(1/2, 1/2, 0)$ and equivalent points in striking contrast to both the DLM calculation results and the experimental data. The ASRO of $Fe_{75}V_{25}$ has also been calculated by Turchi *et al* [33] using the generalized perturbation method based on an electronic structure with no spin polarization to determine the effective pair interactions. If we neglect the PM local exchange splitting and the charge-rearrangement effects, we obtain similar ASRO to that of their data, but this is clearly not representative of the alloy.

In summary, we conclude that the experimental data (although not the fits) are well interpreted by our calculations of ASRO and magnetic correlations. ASRO is evidently strongly affected by the local moments associated with the iron sites in the paramagnetic state, leading to only small differences between the topologies of the ASRO established in samples quenched from above and below T_c. The principal difference is the growth of structure at around $(1/2, 1/2, 1/2)$ for the ferromagnetic state. The ASRO strengthens quite sharply as the system orders magnetically and it would be interesting if an *in situ*, polarized neutron, scattering experiment could be carried out to investigate this.

5. Atomic short-range order of $Fe_{80}Al_{20}$

The technological importance and interplay between magnetism and compositional order described in the introduction have made iron-rich Fe–Al alloys and $Fe_{80}Al_{20}$, in particular, the subjects of a series of x-ray and neutron diffuse scattering experiments. Happily the Fe–Al valence and neutron scattering length differences make **Fe**Al suitable for both types of study.

Epperson and Spruiell [34] investigated the ASRO via x-ray studies on polycrystalline samples with around 25% aluminium, heat treated in a variety of ways and quenched from a range of temperatures. They provided evidence for the tendency to ordering to the DO_3 superstructure. This is characterized by concentration waves with $\boldsymbol{q} = (1, 0, 0)$ and $(1/2, 1/2, 1/2)$. Schweika *et al* [35] carried out an *in situ*, unpolarized, neutron experiment on a single crystal of $Fe_{80}Al_{20}$ at temperatures between 823 K and 1073 K. They made an assessment of the magnetic scattering in the ferromagnetic regime so that they could attempt to isolate the nuclear scattering. They presented data for the ferromagnetic alloy from the $(0, 0, 1)$ and $(2, 1, 1)$ planes at $T = 823$ K and the $(0, 0, 1)$ plane at 923 K, as well as the $(2, 1, 1)$ plane for the paramagnetic alloy at 1073 K. For the ferromagnetic alloy, substantial intensity was found at around $(0, 0, 1)$-equivalent $\boldsymbol{q}$-points which was skewed in the $[1, 1, 1]$ direction, with a possible subsidiary peak at $(1/2, 1/2, 1/2)$. A peculiar feature was noted: that the short-range-order peak at $(1, 0, 0)$ decreased only marginally with increasing temperature from $T = 823$ K to 923 K, which the authors put down to a competition between a Fe–Al chemical interaction and the ferromagnetic coupling between

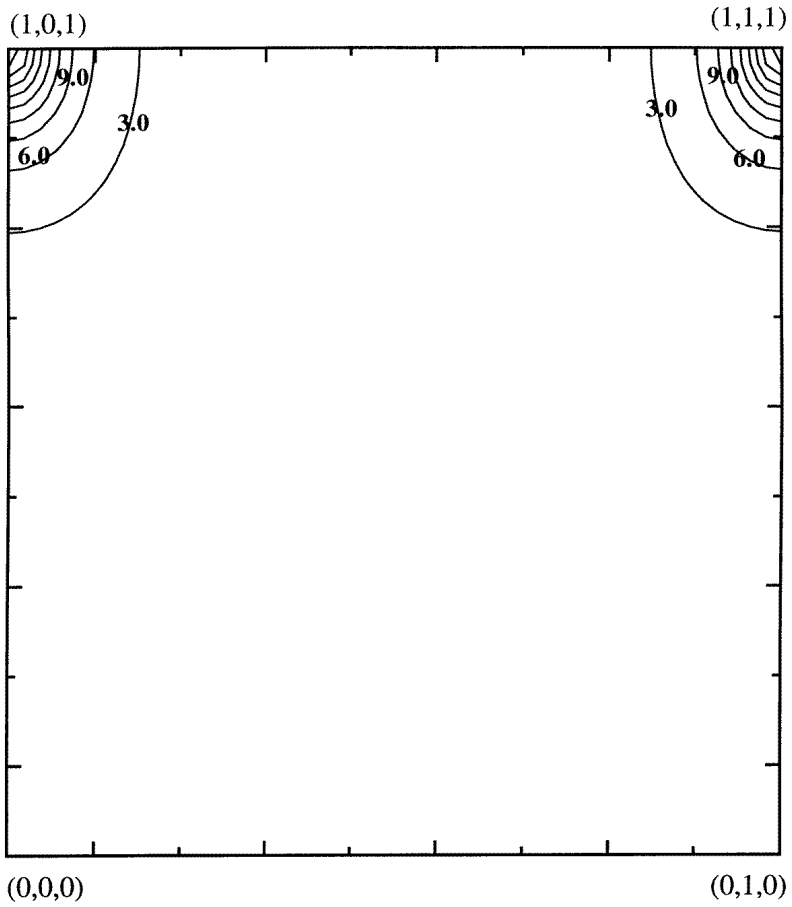

(a)

Figure 5. (a) The ASRO ($\alpha^{DLM}(\boldsymbol{q}, T)$) for the $(1, \bar{1}, 0)$ plane for paramagnetic (DLM) $Fe_{80}Al_{20}$ at 200 K above the theoretical spinodal temperature of 2700 K in Laue units. (b) The ASRO ($\alpha^{DLM}(\boldsymbol{q}, T)$) for the $(1, \bar{1}, 0)$ plane for ferromagnetic $Fe_{80}Al_{20}$ at 1000 K (the theoretical spinodal temperature is 485 K) in Laue units. (c) As (b), but for a lower temperature of 500 K.

Fe moments. From our calculations of the ASRO described below we are able to extract an expression of this effect in terms of the electronic structure. A later paper by Schweika [36] extended the study further to the paramagnetic state, just above the Curie temperature, 935 K. At 1013 K, the scattering intensity from the $(1, \bar{1}, 0)$ plane was found to peak around $(1, 0, 0)$-equivalent points only, but there was also a distortion along $[1, 1, 1]$. Evidence for a phase transition into an ordered phase characterized by $(1/2, 1/2, 1/2)$ concentration wavevectors only at approximately 650 K was also presented. This is consistent with a B32 transient ordered phase observed by Gao and Fultz [37] in $Fe_{75}Al_{25}$.

Pierron-Bohnes *et al* [38] carried out x-ray diffuse scattering measurements on $Fe_{80}Al_{20}$ quenched from 772 K in the ferromagnetic state. They found maximum intensity at $(1, 0, 0)$ and subsidiary peaks at $(1/2, 1/2, 1/2)$ in accord with Schweika *et al*. They complemented this study [39] with diffuse, unpolarized neutron scattering measurements on a single crystal

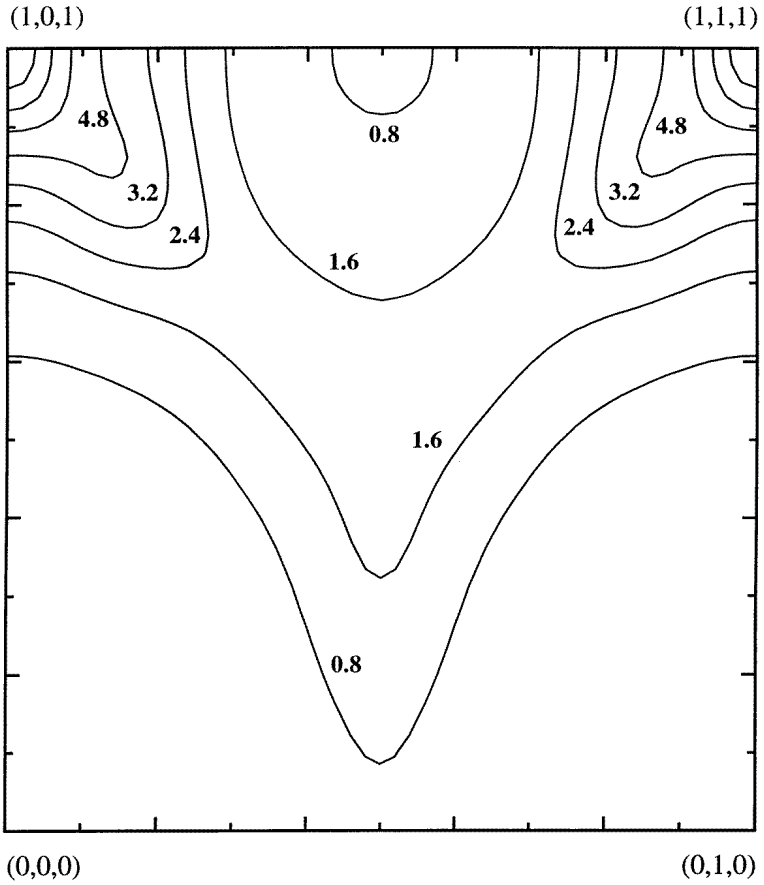

(b)

Figure 5. (Continued)

in situ for several temperatures between 973 K and 1573 K in the paramagnetic regime. Peaks were observed at the $(1, 0, 0)$ points which were slightly elongated along the [1, 1, 1] direction for the lowest temperature of 973 K. No subsidiary peaks were noted at around $(1/2, 1/2, 1/2)$. All of the data seem to show that there is an apparent weakening of the chemical interactions in the ferromagnetic state with a reduced propensity towards B2-type ordering and an increased tendency towards DO_3-type order.

We carried out calculations of the ASRO for both the ferromagnetic and DLM paramagnetic states of $Fe_{80}Al_{20}$. Parallel calculations of $\chi(\boldsymbol{q}, T)$, based on the DLM model, indicated strong ferromagnetic correlations in paramagnetic $Fe_{80}Al_{20}$ and a T_c of 1130 K, in fair agreement with the experimental value of 935 K. Evidently this treatment captures the correct order of magnitude for the energies of the spin fluctuations, just as it does for the elemental metals [18] and **Fe**V. Figures 5(a), 5(b) and 5(c) show the ASRO for both the paramagnetic ($\alpha^{DLM}(\boldsymbol{q}, T)$) and ferromagnetic ($\alpha^{FM}(\boldsymbol{q}, T)$) states of $Fe_{80}Al_{20}$ for the $(1, \bar{1}, 0)$ plane. $\alpha^{DLM}(\boldsymbol{q}, T)$ peaks at $(1, 0, 0)$ showing the same B2-type ASRO as the high-temperature experimental data [39]. In table 2, as was done for Fe–V alloys, we show

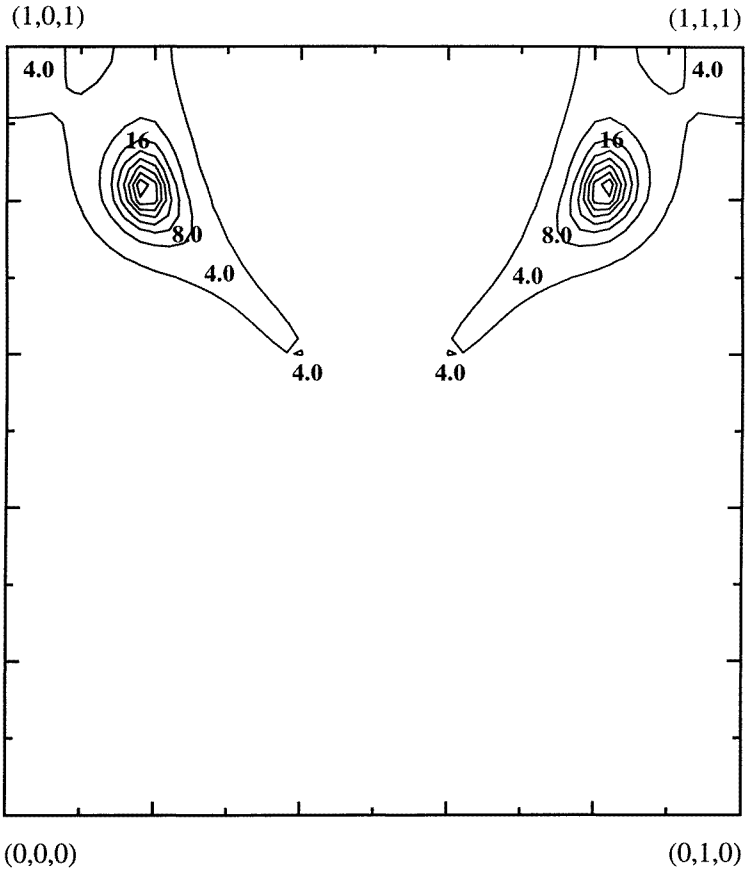

(c)

Figure 5. (Continued)

a real-space representation of the direct correlation function, $S^{(2)}(\boldsymbol{q})$.

$\alpha^{FM}(\boldsymbol{q}, T)$ is presented at two temperatures, one slightly below the Curie temperature at $T = 1000$ K (figure 5(b)) and the other at the lower temperature of 500 K (figure 5(c)). For the higher temperature, $\alpha^{FM}(\boldsymbol{q}, T)$ peaks at $(1, 0, 0)$ with a strong skewing along the $[1, 1, 1]$ direction. This feature is also observed in the experimental data [35]. For the lower temperature, this skewing turns into an incommensurate peak at $(0.8, 0.8, 0.8)$ and there is large intensity from $(0.5, 0.5, 0.5)$ to $(1, 1, 1)$. This latter feature of the calculated $\alpha^{FM}(\boldsymbol{q}, T)$ compares well with that observed for the experimental data [38, 35]. The structure along $[1, 1, 1]$ owes its origin to a Fermi surface effect similar to that which caused the structure around $(1/2, 1/2, 1/2)$ in ferromagnetic $Fe_{87}V_{13}$. It may, therefore, be responsible for the tendency of iron-rich ferromagnetic FeAl alloys to form DO_3 ordered alloys, whereas only B2-type correlations are seen in their paramagnetic states, where local-moment disorder has removed the remnants of sharp structure from the electronic structure at around the Fermi energy. Once again the direct correlation function is fairly long ranged; see table 2 for the $T = 500$ K results.

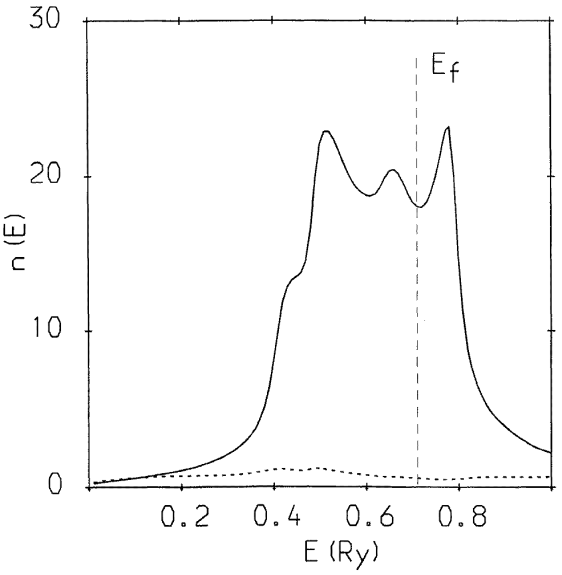

(a)

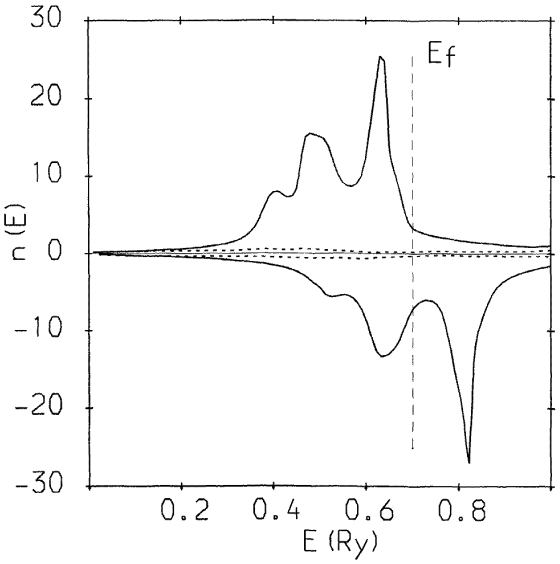

(b)

Figure 6. (a) The compositionally averaged density of states of paramagnetic (DLM) $Fe_{80}Al_{20}$ and its resolution into components associated with Fe (solid) and Al (dotted) sites weighted by concentration, in units of states Ryd^{-1}/(atom spin). (b) The majority- and minority-spin, compositionally averaged densities of states of ferromagnetic $Fe_{80}Al_{20}$ and their resolutions into components weighted by concentration, in units of states Ryd^{-1}/(atom spin). (c) The compositionally averaged density of states of non-magnetic $Fe_{80}Al_{20}$ and its resolution into components associated with Fe (solid) and Al (dotted) sites weighted by concentration, in units of states Ryd^{-1}/(atom spin).

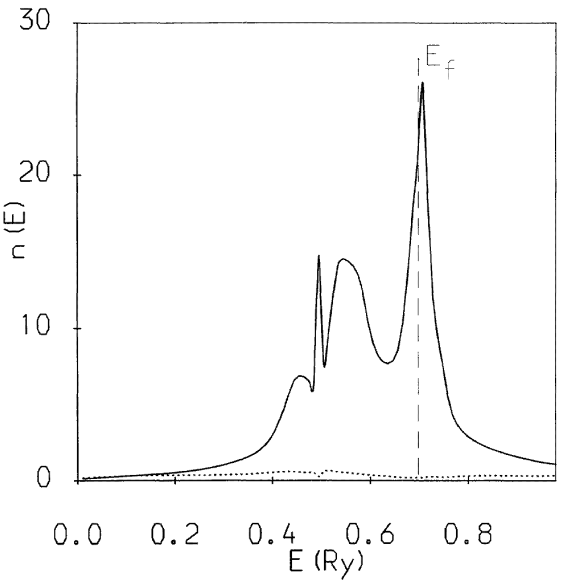

(c)

Figure 6. (Continued)

For the DLM paramagnetic state, a spinodal temperature T_s of 2700 K for a B2 ordering transition is calculated. Even for a mean-field approach, this is a big overestimate. Atomic displacement effects are large in this alloy [40] but have been neglected in our calculations. We would expect the same overall ASRO to be revealed but with a reduced T_s with their inclusion. (Omitting the effects of the Fe local moments from the paramagnetic state increases the ASRO even more, indicating a T_s in excess of 3500 K.) On the other hand, in the ferromagnetic state T_s is 485 K showing that, as in experiment, the compositional correlations weaken as long-range magnetic order is set up. It is useful to understand why this happens from the basis of the underlying 'locally' and 'globally' spin-polarized electronic structures of the paramagnetic and ferromagnetic alloys, respectively [41]. With this insight as a guide, we may make an estimate for the consequence of lattice displacement effects.

When a transition metal (TM) is alloyed with a simple metal, there is a hybridization between the transition metal d and the simple metal p states which creates more tightly bound bonding states together with anti-bonding states at higher energies at the top of the alloy's d-band complex. As discussed in detail by Gelatt *et al* and others [42], not all d states have appropriate symmetry for hybridization, so non-bonding d states are also set up in the alloy with energies close to those in the TM element in between the bonding and anti-bonding p–d states. The alloy has a strong propensity to order if the low-lying bonding states are occupied, so the energy is lowered as the number of unlike nearest neighbours increases. Little further strengthening of this effect occurs if the mid-range, non-bonding states are also occupied; but the tendency is reduced with the occupation of the anti-bonding states. Figures 6(a), 6(b) and 6(c) show the densities of states of paramagnetic (DLM), ferromagnetic (FM) and Stoner paramagnetic (NM) $Fe_{80}Al_{20}$ respectively. Evidently the reason for the local-moment paramagnetic alloy having a strong tendency to order, as shown by $S^{(2)}(\boldsymbol{q})$ and $\alpha^{DLM}(\boldsymbol{q})$ in figure 5(a), traces back to the occupation of the bonding, some non-bonding and

Table 2. As table 1, but for $Fe_{80}Al_{20}$. The fourth column contains interaction parameters extracted by a reciprocal-space analysis of the data obtained by Pierron-Bohnes *et al* [39] for the paramagnetic alloy. The analysis was carried out by Sanchez *et al* [31] who used the CVM. The cube–rhombohedron–octahedron approximation values are quoted. Our calculated ferromagnetic $S_n^{(2)}$s are for two temperatures.

Shells	$S^{(2)}$ FM (1000 K)	$S^{(2)}$ FM (500 K)	$S^{(2)}$ DLM-PM	Sanchez *et al* 1273 K PM
0	−28.5	−33.9	−38.3	
1	−15.5	−14.2	−22.9	−6.96
2	−8.4	−8.1	−5.7	−2.08
3	+ 0.3	+ 0.5	+ 0.3	+ 0.28
4	+ 0.8	+ 1.0	+ 0.2	−0.08
5	+ 0.1	+ 0.0	+ 0.4	−0.48
6	−0.3	−0.3	+ 0.2	—
7	−0.1	−0.1	+ 0.2	—
8	−0.0	−0.0	−0.1	—
9	−0.1	−0.1	—	

only a few anti-bonding states. The unrealistic Stoner paramagnetic state (figure 6(c)) makes this trend stronger; so, with almost no anti-bonding states occupied, the ordering tendency is unphysically large. On the other hand, the 'global' exchange splitting in the electronic structure derived from the long-range magnetic order makes ferromagnetic $Fe_{80}Al_{20}$ a strong ferromagnet with all majority-spin d states, including the anti-bonding states at the top near the Fermi energy, occupied.

We conclude that 'local moments' in the paramagnetic state play an important role in weakening the ordering trend in **Fe**Al alloys as is shown by comparing to the ordering found from a Stoner PM state. For $Fe_{80}Al_{20}$, the lack of 'local exchange splitting' in some regions of $\boldsymbol{k}$- and energy space (figure 6(a) shows this information integrated over $\boldsymbol{k}$-space) has led to fewer filled anti-bonding states than in the ferromagnetic alloy. This is a reason for the relative strength of the compositional correlations in the paramagnetic alloy as compared to those in the ferromagnetic one, counteracting in part the effect of lowering the temperature. Once lattice displacement effects are incorporated into the calculations, we expect an increase in the filling of the anti-bonding states, reducing the strength of the ordering trend. This should occur because the local chemical ordering will lead to a local expansion of the lattice. This will cause a d-band narrowing supporting a more extensive local exchange splitting associated with the iron sites and leading to a greater occupation of anti-bonding states.

6. Conclusions

We have implemented our theory for compositional correlations in metallic alloys for iron-rich FeV and FeAl alloys and have investigated how the ASRO is affected by either the long-range magnetic order in the ferromagnetic states or by the spin fluctuations in the paramagnetic states. The theory is based on a 'first-principles' description of the electronic structure with all-electron effects included. Lattice displacement effects, however, have not been taken into account. A correlated, mean-field theory for both the compositional and magnetic fluctuations which incorporates Onsager cavity fields has been used; this properly obeys the diagonal part of the fluctuation-dissipation theorem, which is not obeyed

in typical applications of mean-field theories. The spin fluctuations of the paramagnetic state are modelled in terms of disordered local moments.

We have compared our calculations of ASRO in detail with diffuse neutron and x-ray scattering experiments and obtain fair agreement although, in the main, the strength of the calculated ASRO for the paramagnetic alloys is somewhat larger than that deduced from experiment. This discrepancy is most likely to be due to the theoretical constraint of a rigid lattice. On the other hand, the estimates of the Curie temperatures agree well with empirical values.

The topology of the ASRO, $\alpha(\boldsymbol{q})$, in $\boldsymbol{q}$-space is accurately described by the theory together with trends which accompany change in the magnetic state and temperature. We have provided an explanation of these features in terms of electronic structure attributes. The relative occupation of bonding and anti-bonding states determined by the 'global' or 'local' exchange splitting has been found to be an important consideration. In both of these iron alloy systems, a Fermi surface effect leads to intensity in $\alpha(\boldsymbol{q})$ at around $(1/2, 1/2, 1/2)$ for the ferromagnetic state which diminishes in the paramagnetic state. We postulate that this is the reason for the tendency for ferromagnetic $Fe_{80}Al_{20}$ alloys to form DO_3 ordered alloys, whilst their paramagnetic counterparts exhibit B2 correlations. These encourage the formation of B2 ordered phases for alloys with more aluminium and therefore lower Curie temperatures.

We suggest that further, polarized, diffuse neutron scattering experiments carried out *in situ* on these alloys would be very desirable. Apart from separating the nuclear scattering cleanly from the magnetic scattering, and, hence, isolating the ASRO, such studies would be able to examine the predicted strengthening and weakening the compositional correlations of $Fe_{87}V_{13}$ and $Fe_{80}Al_{20}$, respectively, as the systems are cooled through their Curie temperatures, as well as examining the development of intensity and structure at around $(1/2, 1/2, 1/2)$. Finally, experiments of this ilk would be of great benefit to our ongoing development of the theory to incorporate lattice displacement effects.

Acknowledgments

This work was supported in part by the EPSRC in the UK and by the US Department of Energy, Office of Basic Energy Sciences, Division of Materials Science, through a New-Initiative Grant under contract No DE-AC04-94AL85000 with Sandia. JBS thanks D McK Paul for useful discussions and B Ginatempo for his help and insight in determining the alloy Fermi surfaces.

References

[1] Mirebeau I, Cadeville M C, Parette G and Campbell I A 1982 *J. Phys. F: Met. Phys.* **12** 25
[2] Cable J W, Child H R and Nakai Y 1989 *Physica* B **156+157** 50
[3] Pierron-Bohnes V, Kentzinger E, Cadeville M C, Sanchez J M, Caudron R, Solal F and Kozubski R 1995 *Phys. Rev.* B **51** 5760
[4] Stephens J R 1987 *High Temperature Ordered Intermetallic Alloys* vol 39, ed C C Koch, C T Liu and N S Stolhoff (Pittsburgh, PA: MRS) p 381
[5] McKamey C G, Devan J H, Tortorelli P F and Sikka V K 1991 *J. Mater. Res.* **6** 1779
[6] Massalski T B, Okamoto H, Subramanian P R and Kacprzak L (ed) 1990 *Binary Alloy Phase Diagrams* 2nd edn (Metals Park, OH: American Society for Metals)
[7] Gubanov V A, Liechtenstein A I and Postnikov A I 1992 *Magnetism and Electronic Structure of Crystals (Springer Series in Solid State Physics 98)* (Berlin: Springer)
[8] Staunton J B 1994 *Rep. Prog. Phys.* **57** 1289
[9] Pettifor D G 1978 *Solid State Commun.* **28** 621

Pettifor D G 1979 *Phys. Rev. Lett.* **42** 846
[10] Heine V and Samson J 1983 *J. Phys. F: Met. Phys.* **13** 2155
[11] Ducastelle F 1989 *Alloy Phase Stability (NATO ASI Series E, vol 163)* ed G M Stocks and A Gonis (Dordrecht: Kluwer) pp 293–328
[12] Williams A R, Moruzzi V L, Gelatt C D and Kubler J 1983 *J. Magn. Magn. Mater.* **31–34** 88
[13] Johnson D D, Pinski F J and Staunton J B 1987 *J. Appl. Phys.* **61** 3715
Johnson D D, Pinski F J, Staunton J B, Gyorffy B L and Stocks G M 1990 *Physical Metallurgy of Controlled Expansion Invar-Type Alloys* ed K C Russell and D F Smith (Pittsburgh, PA: TMMS) pp 3–24
[14] Johnson D D, Pinski F J and Stocks G M 1985 *J. Appl. Phys.* **57** 3018
[15] Staunton J B, Johnson D D and Gyorffy B L 1987 *J. Appl. Phys.* **61** 3693
[16] Moriya T (ed) 1981 *Electronic Correlations and Magnetism in Narrow Band Systems* (Berlin: Springer)
[17] Gyorffy B L, Pindor A J, Staunton J, Stocks G M and Winter H 1985 *J. Phys. F: Met. Phys.* **15** 1337
Staunton J, Gyorffy B L, Stocks G M and Wadsworth J 1986 *J. Phys. F: Met. Phys.* **16** 1761
Staunton J B, Gyorffy B L, Pindor A J, Stocks G M and Winter H 1985 *J. Phys. F: Met. Phys.* **15** 1387
[18] Staunton J B and Gyorffy B L 1992 *Phys. Rev. Lett.* **69** 371
[19] Ling M F, Staunton J B and Johnson D D 1994 *Europhys. Lett.* **25** 631
Ling M F, Staunton J B and Johnson D D 1994 *J. Phys.: Condens. Matter* **6** 6001
[20] Ling M F, Staunton J B and Johnson D D 1994 *J. Phys.: Condens. Matter* **6** 5981
[21] Kisker E, Schroder K, Campagna M and Gudat W 1984 *Phys. Rev. Lett.* **52** 329
Kirschner J, Globl M, Dose V and Scheidt H 1984 *Phys. Rev. Lett.* **53** 612
[22] Haines E M, Clauberg R and Feder R 1985 *Phys. Rev. Lett.* **54** 932
[23] Staunton J B, Johnson D D and Pinski F J 1994 *Phys. Rev.* B **50** 1450
Johnson D D, Staunton J B and Pinski F J 1994 *Phys. Rev.* B **50** 1473
[24] Ling M F, Staunton J B and Johnson D D 1995 *J. Phys.: Condens. Matter* **7** 1863
[25] Khachaturyan A G 1983 *Theory of Structural Transformations in Solids* (Chichester: Wiley) p 39
[26] Gyorffy B L and Stocks G M 1983 *Phys. Rev. Lett.* **50** 374
[27] Schweika W and Haubold H G 1987 *Phys. Rev.* B **36** 3935
[28] Gratias D and Cédédèse P 1985 *J. Physique Coll.* **46** C9 149
[29] Johnson D D and Pinski F J 1993 *Phys. Rev.* B **48** 11 553
[30] Staunton J B, Johnson D D and Pinski F J 1990 *Phys. Rev. Lett.* **65** 1259
[31] Sanchez J M, Pierron-Bohnes V and Mejia-Lira F 1995 *Phys. Rev.* B **51** 3429
[32] It is noteworthy that the inclusion of the effects of Onsager cavity fields into our theory guarantees the equivalence of $\int \alpha(\boldsymbol{q})\, \mathrm{d}\boldsymbol{q}$ to one; see references [18, 23]
[33] Sluiter M and Turchi P E A 1991 *High-Temperature Ordered Intermetallic Alloys IV (MRS Proceedings 313)* ed L A Johnson, D P Pope and J O Stiegler (Pittsburgh, PA: MRS) p 37
Turchi P E A, Reinhard L and Stocks G M 1994 *Phys. Rev.* B **50** 15 542
[34] Epperson J E and Spruiell J E 1969 *J. Phys. Chem. Solids* **30** 1733
[35] Schweika W, Monkenbusch M and Ackermann H 1989 *Physica* B **156+157** 78
[36] Schweika W 1990 *Mater. Res. Soc. Symp. Proc.* **166** 249
[37] Gao Z Q and Fultz B 1993 *Phil. Mag.* B **67** 787
[38] Pierron-Bohnes V, Lefebvre S, Bessiere M and Finel A 1990 *Acta. Metall. Mater.* **38** 2701
[39] Pierron-Bohnes V, Cadeville M C, Finel A and Schaerpf O 1991 *J. Physique* I **1** 247
[40] Anthony L, Nagel L J, Okamoto J K and Fultz B 1994 *Phys. Rev. Lett.* **73** 3034
[41] Ling M F, Staunton J B, Johnson D D and Pinski F J 1995 *Phys. Rev.* B **52** R3816
[42] Gelatt C D, Williams A R and Moruzzi V L 1983 *Phys. Rev.* B **27** 2005
Corb B W, O'Handley C and Grant N J 1983 *Phys. Rev.* B **27** 636